Cancer Immunology, Immunotherapy (2020) 69:1519–1534
https://doi.org/10.1007/s00262-020-02560-5

ORIGINAL ARTICLE

^{18}F-fluorodeoxyglucose positron emission tomography correlates with tumor immunometabolic phenotypes in resected lung cancer

Kyle G. Mitchell[1] · Behrang Amini[2] · Yunfei Wang[3] · Brett W. Carter[2] · Myrna C. B. Godoy[2] · Edwin R. Parra[4] · Carmen Behrens[5] · Pamela Villalobos[4] · Alexandre Reuben[5] · J. Jack Lee[6] · Annikka Weissferdt[7] · Cesar A. Moran[7] · Junya Fujimoto[4] · Boris Sepesi[1] · Garrett L. Walsh[1] · Ara A. Vaporciyan[1] · Wayne L. Hofstetter[1] · William N. William Jr.[5,8] · Don L. Gibbons[5,9] · Jing Wang[10] · Patrick Hwu[3] · Stephen G. Swisher[1] · David Piwnica-Worms[11] · Humam Kadara[4] · Ignacio I. Wistuba[4,5] · John V. Heymach[5] · Weiyi Peng[3,12] · Tina Cascone[5]

Received: 26 September 2019 / Accepted: 31 March 2020 / Published online: 16 April 2020

Abstract

Enhanced tumor glycolytic activity is a mechanism by which tumors induce an immunosuppressive environment to resist adoptive T cell therapy; therefore, methods of assessing intratumoral glycolytic activity are of considerable clinical interest. In this study, we characterized the relationships among tumor ^{18}F-fluorodeoxyglucose (FDG) retention, tumor metabolic and immune phenotypes, and survival in patients with resected non-small cell lung cancer (NSCLC). We retrospectively analyzed tumor preoperative positron emission tomography (PET) ^{18}F-FDG uptake in 59 resected NSCLCs and investigated correlations between PET parameters (SUV_{Max}, SUV_{Total}, SUV_{Mean}, TLG), tumor expression of glycolysis- and immune-related genes, and tumor-associated immune cell densities that were quantified by immunohistochemistry. Tumor glycolysis-associated immune gene signatures were analyzed for associations with survival outcomes. We found that each ^{18}F-FDG PET parameter was positively correlated with tumor expression of glycolysis-related genes. Elevated ^{18}F-FDG SUV_{Max} was more discriminatory of glycolysis-associated changes in tumor immune phenotypes than other ^{18}F-FDG PET parameters. Increased SUV_{Max} was associated with multiple immune factors characteristic of an immunosuppressive and poorly immune infiltrated tumor microenvironment, including elevated PD-L1 expression, reduced $CD57^+$ cell density, and increased T cell exhaustion gene signature. Elevated SUV_{Max} identified immune-related transcriptomic signatures that were associated with enhanced tumor glycolytic gene expression and poor clinical outcomes. Our results suggest that ^{18}F-FDG SUV_{Max} has potential value as a noninvasive, clinical indicator of tumor immunometabolic phenotypes in patients with resectable NSCLC and warrants investigation as a potential predictor of therapeutic response to immune-based treatment strategies.

Keywords Resected non-small cell lung cancer · Positron emission tomography · Tumor immunometabolic phenotypes · Tumor glycolysis

Abbreviations

^{18}F-FDG	^{18}F-fluorodeoxyglucose
CI	Confidence interval
CT	Computed tomography
DFS	Disease-free survival
DISTHG	Downregulated Immune Signature of Tumors with High Glycolysis
FFPE	Formalin-fixed, paraffin-embedded
HR	Hazard ratio
ICI	Immune checkpoint inhibitor
IHC	Immunohistochemistry
IQR	Interquartile range
NSCLC	Non-small cell lung cancer
OS	Overall survival
PET	Positron emission tomography
PROSPECT	Profiling of Resistance Patterns and Oncogenic Signaling Pathways in Evaluation of Cancers of the Thorax
SUV	Standardized uptake value

Electronic supplementary material The online version of this article (https://doi.org/10.1007/s00262-020-02560-5) contains supplementary material, which is available to authorized users.

✉ Weiyi Peng
wpeng2@central.uh.edu

✉ Tina Cascone
tcascone@mdanderson.org

Extended author information available on the last page of the article

TAIC	Tumor-associated immune cell
TLG	Total lesion glycolysis
UISTHG	Upregulated Immune Signature of Tumors with High Glycolysis
VOI	Volume of interest

Introduction

Recent success in the treatment of locally advanced and metastatic non-small cell lung cancer (NSCLC) with immunotherapy has provided a paradigm shift in the management of this disease [1–4]. Unfortunately, however, many patients with NSCLC are refractory to immune-based therapies and the processes by which tumors evade the immune system and become resistant to therapy have not been fully elucidated. Much recent effort has been directed toward the development of clinical methods that may provide tumor- and immune-related information that could inform treatment decisions and maximize the clinical effectiveness of immunotherapy.

Accumulating evidence suggests that tumor metabolism may play a critical role in determining tumor progression and response to immune-based therapies. The activation of oncogenic signaling pathways (e.g., mTOR, BRAF, etc.) has been shown to enhance cancer cell glycolysis and lead to accumulation of lactate in the tumor microenvironment and local immunosuppression [5]. Glucose consumption by tumors may have a detrimental impact on an antitumor immune response by dampening T cell mTOR activity, glycolytic capacity, and IFN-γ production [6]. In addition, acidification of the tumor microenvironment further impairs T cell function [7], drives cancer cell invasion [8], and, moreover, predicts likelihood of metastases, tumor recurrence, and poor patient outcomes [9]. Recently, we reported that tumor glycolysis may impair T cell trafficking and effector functions in human NSCLC and melanoma and that glycolytic end products contribute to resistance of melanoma to T cell-induced killing [10]. However, the approaches used in these studies to characterize the tumor metabolic phenotype have limited clinical applicability.

^{18}F-fluorodeoxyglucose (FDG) positron emission tomography (PET) measures the uptake of radiolabeled ^{18}F-FDG by cells and provides an accurate and noninvasive method to evaluate pulmonary nodules and masses. PET may also be used to guide cancer staging, facilitate the decision-making process, and to quantify responses to therapy [11]. Pretreatment ^{18}F-FDG retention has been shown to have prognostic value for a number of malignancies, including NSCLC [11–14]. By measuring the level of uptake by cancer cells of a radiolabeled glucose analog, ^{18}F-FDG PET has appeal as a readily available clinical method for the functional evaluation of tumor burden, providing important information that can influence the management of several aspects of the disease and guide therapy [15]. However, whether analysis of tumor metabolic phenotypes using ^{18}F-FDG PET provides additional clinical utility remains under investigation.

Here, we investigated whether preoperative ^{18}F-FDG retention is associated with tumor glycolytic gene expression and tumor immune phenotypes in patients with operable early-stage/locally advanced NSCLC. We also determined whether ^{18}F-FDG PET metabolic parameters can be used to identify patients with resectable NSCLC who are at high risk of poor postoperative survival. To test this, we retrospectively examined preoperative ^{18}F-FDG PET parameters, overall tumor expression of glycolysis-related genes in cancer cells and other cell populations within the tumor microenvironment, and immune cell infiltration of tumors in patients who underwent surgical resection of NSCLC.

Materials and methods

Study design, population, and treatment

Patients were considered eligible for analysis if they underwent resection of primary NSCLC (stages I–III) at the University of Texas MD Anderson Cancer Center and were enrolled in the Profiling of Resistance Patterns and Oncogenic Signaling Pathways in Evaluation of Cancers of the Thorax (PROSPECT) study, which has the benefits of full clinical annotation, detailed immune profiling, and long postoperative follow-up [10, 16–18]. To limit potential temporal changes in tumor biology from the time of ^{18}F-FDG PET to that of resection, only patients who underwent PET/computed tomography (CT) within 30 days prior to surgical tumor resection were included (Supplementary Fig. 1) [19]. Postoperatively, all patients underwent periodic surveillance in accordance with guidelines in effect at the time of treatment. All tumors were retrospectively staged using the seventh edition of the International Association for the Study of Lung Cancer staging system [20].

Image acquisition and analysis

All images were obtained using a dedicated PET/CT system (Discovery ST, STe, or RX; GE Medical Systems and GE Healthcare). After fasting for a minimum of 6 h and undergoing confirmation of a blood glucose level less than 200 mg/dL, patients received an intravenous infusion of 259–740 MBq^{18}F-FDG. A CT scan was performed for anatomic correlation and attenuation correction; PET images were subsequently obtained 60–90 min after ^{18}F-FDG infusion. All images were retrospectively reviewed by an experienced board-certified radiologist (B. Amini) who was

blinded to the patients' clinicopathologic characteristics and outcomes. Regions of interest and volumes of interest (VOIs) were identified as pathologic areas on imaging with ^{18}F-FDG uptake exceeding that of the background and segmented using a semiautomated spatial derivative contouring algorithm (MIMVista version 6.6; MIM software) with high accuracy and reproducibility [21, 22]. This contouring method has been validated in a multi-observer study that showed superiority over manual and threshold methods [22]. The maximum standardized uptake value (SUV_{Max}) was defined as the greatest uptake in a single voxel within the semiautomatically defined VOI. The total SUV (SUV_{Total}) was calculated as the sum of the SUV throughout the VOI, and the mean SUV (SUV_{Mean}) was defined as the average SUV throughout the VOI. Total lesion glycolysis (TLG) was calculated as the product of the SUV_{Mean} and active tumor volume within the VOI.

mRNA extraction and transcriptomic analysis

To delineate the relationship between ^{18}F-FDG PET metabolic parameters and tumor glycolytic gene expression, expression of 18 genes (*ALDOA*, *ALDOC*, *BPGM*, *ENO2*, *ENO3*, *FBP1*, *FBP2*, *GAPDH*, *GPI*, *LDHA*, *LDHB*, *PFKM*, *PFKP*, *PGAM1*, *PGAM4*, *PGK1*, *PGK2, SLC2A1*) involved in the glycolytic pathway was quantified in resected NSCLC tumors [10]. These genes were selected for analysis because our group previously identified their expression to be correlated with tumor immune markers in resected NSCLCs [10]. mRNA was extracted from formalin-fixed, paraffin-embedded (FFPE) NSCLC tumor tissues, and gene expression was quantified using an Illumina Human WG-6 v3 BeadChip according to previously described methods [16–18]. Microarray data have been previously deposited and are publicly available (Gene Expression Omnibus, GSE42127) [10, 16–18, 23]. A signature of overall tumor expression of glycolysis-related genes was defined as the geometric mean expression level of the representative genes *GPI* and *PGAM4*, which we have previously shown to be well correlated with increased tumor intrinsic glycolytic activity according to analysis of bioenergetic profiles of tumor cell lines [10]. To further characterize immune phenotypic changes associated with tumor glycolytic metabolism, we analyzed expression of 708 genes well recognized as having roles in antitumor immunity [24]. Pairwise associations between expression of these 708 genes with ^{18}F-FDG PET parameters and overall tumor expression of glycolytic genes were analyzed using Pearson's correlations, with adjustments for multiple comparisons using the Benjamini–Hochberg method [25]. Gene dysregulation analysis was performed using the R package *limma* [26] to identify differentially expressed genes (|log-fold change|> 1, $P < 0.05$) according to each parameter (overall tumor glycolysis gene expression, SUV_{Max}, SUV_{Mean}, SUV_{Total}, TLG). Transcriptomic data were additionally analyzed using Ingenuity Pathway Analysis (QIAGEN Inc) [27], with significantly dysregulated pathways defined as $|z\ score| \geq 1.5$ and $-\log_{10}(P\text{-value}) \geq 2$. To define transcriptomic profiles indicative of exhausted T cell phenotypes, we used two gene signatures: the mean expression levels of a subset of genes in the pan-cancer Tumor Inflammation Signature (*TIGIT*, *LAG3*, *CD274*, *PDCD1LG2*, *CD276*) [28], and the mean expression level of *CTLA4*, *HAVCR2*, *LAG3*, *PDCD1*, and *TIGIT* [29].

Immunohistochemical analysis of immune cell infiltration of tumors

Immunohistochemical staining was performed using an automated staining system (BOND-MAX; Leica Microsystems) with 4-µm-thick sequential histologic tumor sections of FFPE tumor samples with antibodies against CD3, CD4, CD8, CD57, GZB, CD45RO, FOXP3, CD68, and PD-L1 [10, 30, 31]. Expression of all cell markers was detected using a Novocastra Bond Polymer Refine Detection kit (Leica Microsystems) with a diaminobenzidine reaction to identify antibody labeling and hematoxylin counterstaining. At the same time, tonsil tissue samples were analyzed as positive controls according to the same protocol; negative controls were incubated without primary antibodies.

Slides containing whole tumor sections were digitally scanned at 200× magnification using a ScanScope Aperio AT Turbo slide scanner (Leica Microsystems) and visualized using the ImageScope software program (Leica Microsystems). Tumor-associated immune cells (TAICs) expressing CD3, CD4, CD8, CD57, GZB, CD45RO, FOXP3, or CD68 were evaluated by counting positive cells in five square areas (1 mm^2 each) in the intratumoral compartment, using a nuclear algorithm to identify subpopulations of lymphocytes and a cytoplasmic algorithm to identify macrophages. Each area examined was overlapped with sequential immunohistochemical slides to quantify each marker at the same location of the tumor. The average total number of immune cells positive for each marker in the five square areas was expressed as immune cell density (number of cells/mm^2) [30, 31]. A cellular membrane detection algorithm was used to identify expression of PD-L1 by malignant cells using methods that have been described previously; PD-L1 expression was subsequently quantified as an *H*-score (product of staining intensity [range 0–3+] and percentage of cells expressing PD-L1 [range 0–100]; possible range 0–300) [30].

Statistics

Pairwise associations among ^{18}F-FDG PET parameters, tumor expression of glycolysis-related genes, and TAIC densities were analyzed using Pearson correlation coefficients

after $\log_2$ transformation of all values. Differences in continuous variables between groups were analyzed using unpaired *t* tests. Overall survival (OS) was defined as the time from surgical tumor resection to death due to any cause; patients alive at last follow-up were censored on the date of last contact. Disease-free survival (DFS) was defined as the time from resection to recurrence or death; patients without a DFS event were censored on the date of last contact. Survival was estimated using the Kaplan–Meier method, and differences between groups in time-to-event outcomes were analyzed using the log-rank test. For identification of the transcriptomic Upregulated Immune Signature of Tumors with High Glycolysis (UISTHG), genes were selected if they were significantly upregulated (log-fold change > 1, $P < 0.05$) according to elevated (> median) overall tumor glycolytic gene expression and were associated with OS (univariable Cox false discovery rate-adjusted $P < 0.10$). The Downregulated Immune Signature of Tumors with High Glycolysis (DISTHG) included genes that were significantly downregulated (log-fold change < − 1, $P < 0.05$) according to elevated (> median) overall tumor glycolytic gene expression and were associated with OS (univariable Cox false discovery rate-adjusted $P < 0.10$). UISTHG and DISTHG were defined as the mean overall expression of their constituent genes, and the cohort was dichotomized according to the median expression level of each signature. Given the number of observed events in the study cohort, multivariable Cox analysis in the PROSPECT cohort was restricted to adjustment for pathologic stage, histology, and receipt of neoadjuvant and/or adjuvant platinum-based chemotherapy in order to avoid model overfitting. For validation of these signatures, we analyzed publicly available transcriptomic data [32] via a web-based tool (https://kmplot.com/analysis). For these analyses, UISTHG and DISTHG gene expression signatures were again defined as the mean expression level of their constituent genes and dichotomized according to the observed median. Multivariable OS analyses were performed with adjustment for stage and histology among the samples with such data available. Statistical significance was defined as a two-tailed *P* value less than 0.05. All statistical analyses were performed using Python (version 2.7; Python Software Foundation; *seaborn* [0.8.1] package was used for plotting) and R [33].

Results

Patient characteristics

We identified 172 patients with stage I-III NSCLC in the cohort who underwent curative-intent surgery, 123 (72%) of whom had preoperative ^{18}F-FDG PET and available tumor microarray data (Supplementary Fig. 1). Of these patients, we included 59 (48%) who underwent PET within 30 days prior to surgery in the present study (median delay from PET to resection 16.0 days, interquartile range [IQR] 12.0–24.0 days). The clinicopathologic and treatment characteristics of these 59 patients are shown in Supplementary Table 1. Of the patients eligible for analysis, most were men, white, former or current smokers, and treatment-naïve. Adenocarcinomas and early-stage tumors constituted the majority of the tumors examined. Pairwise correlation analysis showed that SUV_{Max}, SUV_{Mean}, SUV_{Total}, and TLG parameters were positively correlated among each other (Fig. 1a, b), with the strongest magnitudes of correlation (as measured by Pearson correlation coefficient) observed between parameters measuring the intensity of tumor ^{18}F-FDG uptake (SUV_{Max} and SUV_{Mean}, $r = 0.953$) and between those reflecting overall tumor burden (SUV_{Total} and TLG, $r = 0.995$).

^{18}F-FDG PET parameters correlate with transcriptomic quantification of tumor glycolytic gene expression

To investigate whether ^{18}F-FDG PET parameters are clinical indicators of tumor glycolytic metabolism, we first examined the association of the ^{18}F-FDG PET parameters with the expression of 18 glycolysis-related genes in tumor tissues from patients with NSCLC. We found that all four parameters were significantly positively correlated with elevated expression levels of glycolysis-related genes, including *ALDOA*, *ALDOC*, *GAPDH*, *GPI*, *LDHA*, *PFKM*, *PFKP*, *PGAM1*, *PGAM4*, *PGK1*, and *SLC2A1* (Fig. 1c, d). We also observed a significant negative correlation between preoperative tumor ^{18}F-FDG retention and the expression of fructose-1,6-bisphosphatase 1 (*FBP1*), which opposes glycolysis and pyruvate production by catalyzing the conversion of fructose-1,6-bisphosphate to fructose-6-phosphate. We further stratified our cohort based on their histotype and found a similar positive correlation between the expression of glycolysis-related genes and FDG retention parameters in patient with lung adenocarcinomas ($n = 43/59$, Supplementary Table 1; data not shown). Due to limitations imposed by the small sample size of patients with squamous cell carcinomas ($n = 16/59$, Supplementary Table 1), the stratified analyses among this subgroup were underpowered to make definitive conclusions (data not shown). By analyzing bioenergetic profiles of cancer cell lines, we previously demonstrated that elevated overall tumor expression of glycolysis-related genes, defined as the mean expression level of the representative genes *GPI* and *PGAM4*, is correlated with increased tumor intrinsic glycolytic activity [10]. To examine whether the ^{18}F-FDG PET parameters could be potential clinical indicators of overall tumor glycolysis, we tested correlations between PET parameters and overall glycolytic

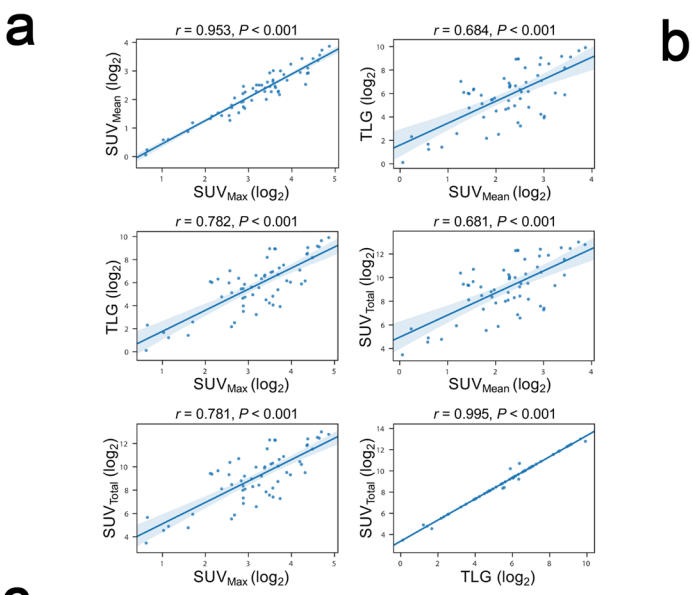

b

	SUV_{Max}	SUV_{Mean}	TLG	SUV_{Total}
SUV_{Max}	1.000	0.953	0.782	0.781
SUV_{Mean}	0.953	1.000	0.684	0.681
TLG	0.782	0.684	1.000	0.995
SUV_{Total}	0.781	0.681	0.995	1.000

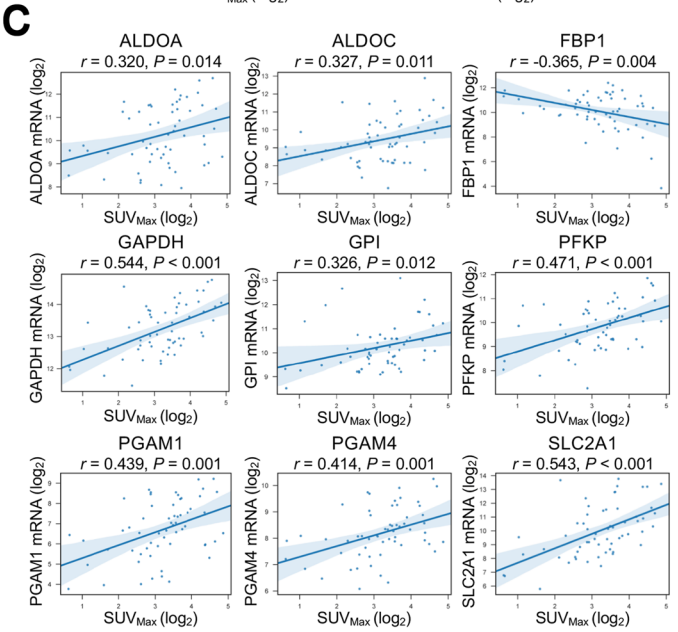

d

	SUV_{Max}	SUV_{Mean}	TLG	SUV_{Total}
ALDOA	0.320	0.239	0.416	0.430
ALDOC	0.327	0.301	0.280	0.282
BPGM				
ENO2			0.230	0.251
ENO3				
FBP1	-0.365	-0.367	-0.324	-0.299
FBP2				
GAPDH	0.544	0.481	0.549	0.560
GPI	0.326	0.283	0.373	0.389
LDHA	0.289	0.238		0.223
LDHB				
PFKM			0.280	0.281
PFKP	0.471	0.428	0.445	0.458
PGAM1	0.439	0.365	0.417	0.415
PGAM4	0.414	0.339	0.400	0.399
PGK1	0.362	0.319	0.297	0.305
PGK2				
SLC2A1	0.543	0.463	0.588	0.583

Fig. 1 Preoperative tumor ^{18}F-FDG uptake is associated with expression of genes encoding enzymes associated with glycolysis ($n=59$). **a**, **b** Positive correlations between parameters measuring the intensity of tumor ^{18}F-FDG uptake (SUV_{Max} and SUV_{Mean}) and those reflecting tumor burden (SUV_{Total} and TLG). All ^{18}F-FDG PET parameters were $\log_2$-transformed. The values provided are Pearson correlation coefficients; a two-tailed P value less than 0.05 was used to determine significance. Blue cells in b reflect statistically significant positive correlations; the intensity of cell color is scaled to the magnitude of the Pearson correlation coefficient. **c** Correlations of expression of glycolysis-related genes with preoperative SUV_{Max}. **d** Statistically significant positive (blue) and negative (red) correlations of expression of glycolysis-related genes with four semiquantitative ^{18}F-FDG PET parameters. mRNA expression and all^{18}F-FDG PET parameters were $\log_2$-transformed. The values provided in a-d are Pearson correlation coefficients; a two-tailed P value less than 0.05 was used to determine significance. The gray cells in d represent absence of a statistically significant correlation. Trends towards positive correlations ($0.05 \le P < 0.10$) are depicted as gray cells labeled with Pearson correlation coefficients. *ALDOA* and *ALDOC*, aldolase A and C; *BPGM*, bisphosphoglycerate mutase; *ENO2* and *ENO3*, enolase 2 and 3; *FBP1* and *FBP2*, fructose-1,6-bisphosphatase 1 and 2; *GAPDH*, glyceraldehyde-3-phosphate dehydrogenase; *GPI*, glucose-6-phosphate isomerase; *LDHA* and *LDHB*, lactate dehydrogenase A and B; *PFKM*, phosphofructokinase, muscle; *PFKP*, phosphofructokinase, platelet; *PGAM1* and *PGAM4*, phosphoglycerate mutase family members 1 and 4; *PGK1* and *PGK2*, phosphoglycerate kinase 1 and 2; *SCL2A1*, solute carrier family 2 member 1

gene expression (bulk transcripts from both cancer and other components within the tumor microenvironment) (Fig. 2a–d). These analyses revealed positive correlations between all four ^{18}F-FDG PET parameters and the overall glycolytic gene expression (SUV_{Max}: $r=0.442$, $P<0.001$; SUV_{Mean}: $r=0.371$, $P=0.004$; TLG: $r=0.461$, $P<0.001$;

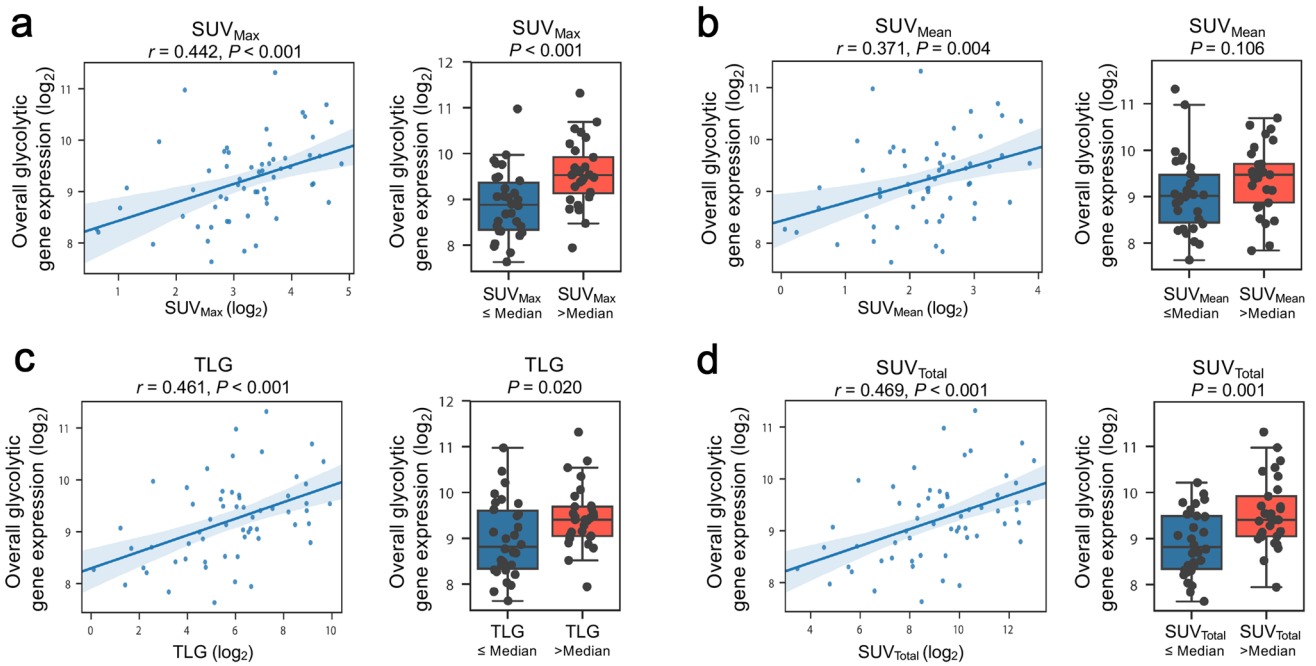

Fig. 2 Correlations between overall tumor expression of glycolysis-related genes and tumor ^{18}F-FDG retention according to **a** SUV_{Max}, **b** SUV_{Mean}, **c** TLG, **d** SUV_{Total} ($n = 59$). Overall tumor expression of glycolytic genes was quantified as the geometric mean of *GPI* and *PGAM4* levels (log_2-transformed); the ^{18}F-FDG PET parameters were similarly log_2-transformed. The values provided in the left panels are Pearson correlation coefficients; a two-tailed *P* value of less than 0.05 was used to determine significance. In the right panels, the cohort was dichotomized according to the observed median of each ^{18}F-FDG PET parameter (SUV_{Max}, 10.36; SUV_{Total}, 643.26; TLG, 64.72; SUV_{Mean}, 4.90). Boxes depict median and interquartile range (IQR); bars represent minimum and maximum values excluding outliers (median ± 1.5 IQR). *P* values in the right panels were calculated using unpaired *t* tests after log_2 transformation of glycolytic gene expression levels. *GPI*, glucose-6-phosphate isomerase; *PGAM4*, phosphoglycerate mutase family member 4

SUV_{Total}: $r = 0.469$, $P < 0.001$). Collectively, these findings suggest that ^{18}F-FDG PET analysis may also provide valuable information regarding glycolytic metabolic phenotypes of tumors from patients with resectable NSCLC.

Preoperative SUV_{Max} discriminates tumor glycolytic phenotypes and is associated with tumor expression of immune-associated genes

After having established that preoperative ^{18}F-FDG PET parameters are clinical indicators of tumor bulk glycolytic metabolism, we next performed correlative analyses to evaluate whether tumor glycolysis, as determined by evaluation of ^{18}F-FDG PET parameters, is associated with changes in expression of genes involved in an antitumor immune response. Our pairwise correlative analyses between the expression of overall tumor glycolytic genes analyzed from the bulk transcriptome and a panel of 708 immune-related genes [24] identified significant associations with increased mRNA levels of 33 genes (Pearson's $r > 0.0$, FDR-adjusted $P < 0.05$) and reduced expression of 51 genes ($r < 0.0$, FDR-adjusted $P < 0.05$) in tumors with high glycolytic gene expression (Fig. 3a, Supplementary Table 2), suggesting that enhanced tumor glycolytic metabolism is associated with immune-related transcriptomic changes in the tumor microenvironment. Next, we sought to identify whether any of the ^{18}F-FDG PET parameters SUV_{Max}, SUV_{Mean}, SUV_{Total}, and TLG was a stronger indicator of tumor–glycolysis-associated changes in immune gene expression. We found that preoperative SUV_{Max} had the greatest number of significant pairwise correlations with immune-related genes (9 positively associated [correlation coefficient range $r = 0.421$–0.543], 12 negatively associated [correlation coefficient range $r = -0.407$ to -0.548] (Fig. 3b; Supplementary Table 3), whereas SUV_{Mean} (15 total genes), SUV_{Total} (6 total genes), and TLG (3 total genes) had fewer individual associations with gene expression (Supplementary Tables 4–6). Moreover, the number of identified overlapping genes significantly associated with glycolytic gene expression was the greatest with SUV_{Max} (12 genes [Fig. 3c–e, SUV_{Max} positive correlation coefficient range $r = 0.421$–0.543, SUV_{Max} negative correlation coefficient range $r = -0.412$ to -0.457] versus SUV_{Mean} [6 genes], SUV_{Total} [3 genes], and TLG [0 genes]).

To confirm the findings from the correlative analyses, we next compared the expression of 708 immune-related genes [24] between high and low glycolytic tumors and identified differentially expressed immune-related genes in

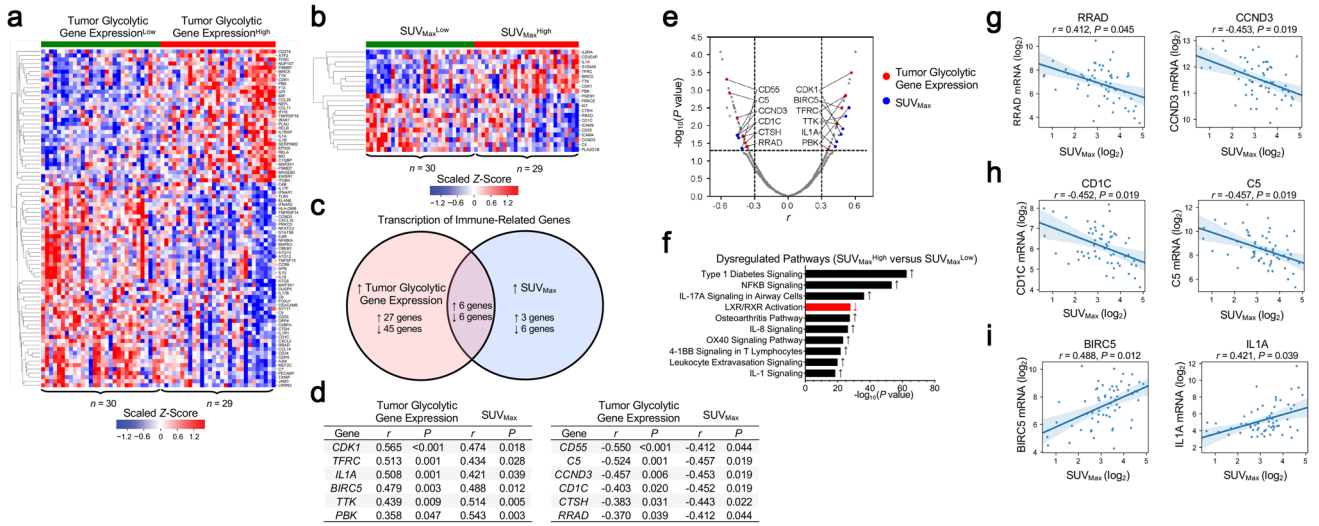

Fig. 3 Preoperative semiquantitative SUV_{Max} identifies changes in transcription of immune-related genes in high and low glycolytic tumors ($n = 59$). **a** Hierarchical clustering of immune-related genes that were most strongly associated (|Pearson's $r| \geq 0.3$, false discovery rate [FDR]-adjusted $P < 0.05$) with enhanced overall tumor expression of glycolysis genes. **b** Hierarchical clustering of immune-related genes associated with preoperative SUV_{Max} according to the same criteria. **c** Venn diagram depicting the overlap in genes that were significantly correlated (FDR-adjusted $P < 0.05$) with overall tumor expression of glycolysis-associated genes and with SUV_{Max}. **d**, **e** Genes that were significantly correlated (FDR-adjusted $P < 0.05$) with tumor glycolytic gene expression and SUV_{Max}. **f** The ten most highly upregulated (black, upward arrow) and downregulated (red, downward arrow) gene signaling pathways among tumors with elevated (> median) SUV_{Max}. **g-i** Associations between preoperative SUV_{Max} and expression of selected genes in resected NSCLC tumors. For **a** and **b**, the study cohort was dichotomized according to the observed median of overall tumor glycolysis gene expression (9.16, **a**) and SUV_{Max} (10.36, **b**). The values provided in **d**, **e**, and **g**–**i** are Pearson coefficients for pairwise correlations between $\log_2$-transformed values; a two-tailed FDR-adjusted P value of less than 0.05 was used to determine significance. For f, dysregulated pathways ($|z\text{-score}| \geq 1.5$, $-\log_{10}[P\text{-value}] \geq 2$ according to Ingenuity Pathway Analysis) were ranked in descending order by $-\log_{10}(P\text{-value})$. *BIRC5*, baculoviral IAP repeat containing 5; *C5*, complement C5; *CCND3*, cyclin D3; *CD1C*, CD1c molecule; *CD55*, CD55 molecule (Cromer blood group); *CDK1*, cyclin-dependent kinase 1; *CTSH*, cathepsin H; *IL1A*, interleukin 1 alpha; *PBK*, PDZ binding kinase; *RRAD*, Ras-related glycolysis inhibitor and calcium channel regulator; *TFRC*, transferrin receptor; *TTK*, TTK protein kinase

these two groups. Using overall tumor bulk glycolytic gene expression to dichotomize our study cohort, we identified 25 differentially expressed immune-related genes (|log-fold change| > 1, $P < 0.05$; 15 genes upregulated, 10 downregulated; Supplementary Table 7). When we dichotomized our study cohort according to SUV_{Max}, we observed 11 total dysregulated genes (Supplementary Table 8; concordance in classification of tumors between overall tumor glycolytic gene expression and SUV_{Max} provided in Supplementary Table 9). Moreover, SUV_{Max} was a more discriminatory indicator of gene dysregulation than SUV_{Mean} (10 genes), SUV_{Total} (5 genes), and TLG (1 gene), and had the greatest overlap of dysregulated genes with tumor bulk glycolytic gene expression (SUV_{Mean}, SUV_{Total}, TLG, Supplementary Table 10). Taken together, our findings suggest that preoperative SUV_{Max} was more discriminatory of glycolysis-associated changes in tumor immune phenotypes than the other ^{18}F-FDG PET parameters.

Examination of the most highly dysregulated pathways in tumors with elevated SUV_{Max} suggested upregulation of several genes known to be involved in proinflammatory signaling (Fig. 3f), including *IL-17A* [34, 35], *IL-8* [36], and *NF-κB* [37]. Examination of the 12 genes that were significantly correlated with both tumor glycolytic gene expression and SUV_{Max} revealed that highly glycolytic tumors were associated with reduced expression of *RRAD*, a negative regulator of tumor aerobic glycolysis [38], and *CCND3*, which shunts glycolytic intermediates toward other metabolic pathways [39] (Fig. 3g). We also observed decreased expression of *CD1C* and *C5*, which are involved in antigen presentation and complement activation, respectively, in highly glycolytic tumors (Fig. 3h). Other shared genes suggested that tumors with high glycolytic gene expression and elevated SUV_{Max} were potentially enriched in molecules involved in cell proliferation and proinflammatory signals, including *BIRC5* and *IL1A* (Fig. 3i). Together, these analyses suggest that assessment of tumor ^{18}F-FDG uptake by SUV_{Max} correlates with tumor immunometabolic changes associated with enhanced tumor glycolytic gene expression. Moreover, these results suggest that resected NSCLC tumors with enhanced ^{18}F-FDG retention are potentially characterized by overexpression of factors involved in tumor progression, local inflammation, and cell cycle dysregulation.

Elevated tumor glycolytic activity as assessed by SUV_{Max} is associated with enhanced expression of PD-L1 and an immunosuppressive phenotype

To further confirm the correlations between preoperative SUV_{Max} and tumor immune phenotypes, we determined the associations between SUV_{Max} and the expression of other immune markers using immunohistochemistry (IHC). Previous reports demonstrated that tumor glycolytic metabolism and PD-L1 expression are tightly interlinked [6]. We next asked whether enhanced expression of PD-L1 may be associated with immune evasion within highly glycolytic NSCLC tumors. Transcriptomic analysis of PD-L1 expression (*CD274* mRNA) demonstrated statistically significant positive associations with overall tumor bulk glycolytic gene expression (Fig. 4a) and SUV_{Max} (Fig. 4b), indicating that ^{18}F-FDG quantification of tumor bulk glycolysis correlates with enhanced tumor expression of PD-L1.

To validate our results at the protein level, we quantified PD-L1 expression using IHC. We noted positive correlations between PD-L1 and increased tumor bulk glycolytic gene expression (Fig. 4c) and with ^{18}F-FDG uptake SUV_{Max} (Fig. 4d). Next, we analyzed correlations between tumor PD-L1 protein levels and expression of 18 glycolysis-related

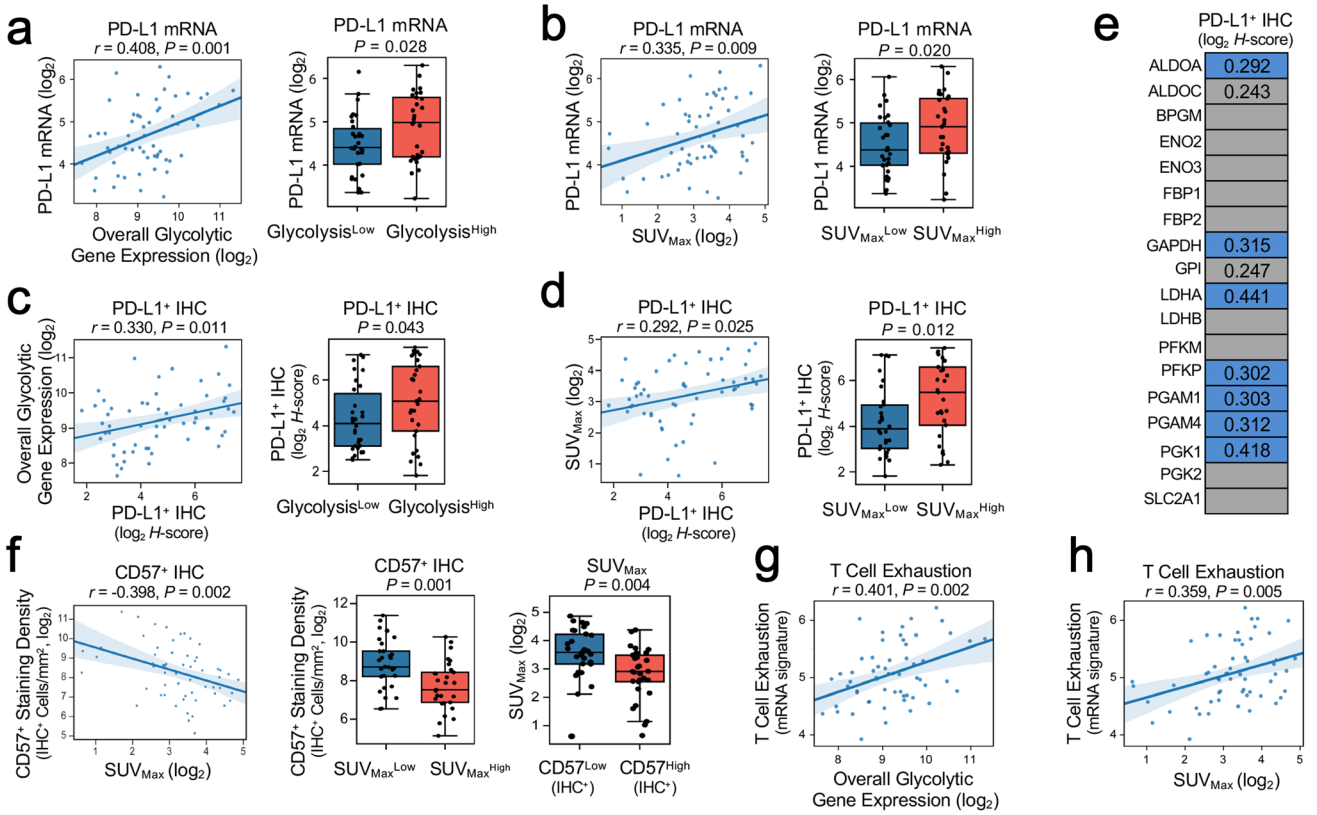

Fig. 4 Elevated tumor glycolytic activity as assessed by SUV_{Max} is associated with enhanced PD-L1 expression and an immunosuppressive phenotype ($n=59$). **a**, **b** Associations between transcription of PD-L1 (*CD274* mRNA) with (a, left and right panels) overall tumor glycolysis and (b, left and right panels) preoperative SUV_{Max}. **c**, **d** Associations between tumor expression of PD-L1 (IHC *H*-score, log_2-transformed) with (c, left and right panels) overall tumor expression of glycolytic genes and (d, left and right panels) SUV_{Max}. **e** Pairwise correlations between tumor PD-L1 IHC H-score (log_2-transformed) and expression of individual glycolytic genes. **f** Elevated preoperative SUV_{Max} was associated with reduced intratumoral infiltration by $CD57^+$ immune cells. **g** The association between overall tumor glycolytic gene expression and an exhausted T cell gene signature (mean expression of *TIGIT*, *LAG3*, *CD274*, *PDCD1LG2*, and *CD276*). **h** The association between SUV_{Max} and exhausted T cell gene signature. Pearson coefficients for pairwise correlations between log_2-transformed values are listed; a two-tailed *P* value of less than 0.05 was used to determine significance. In a-d (right panels) and f (center and right panels), the study cohort is dichotomized according to the observed median of each variable (SUV_{Max}, 10.36; CD57, 330.4 IHC^+ cells/mm^2; overall tumor expression of glycolytic genes, 9.16). Boxes depict median and interquartile range (IQR); bars represent minimum and maximum values excluding outliers (median ± 1.5 IQR). *P* values in the right panels were calculated using unpaired *t* tests. In **e**, the values provided are Pearson correlation coefficients for statistically significant (two-tailed $P<0.05$, blue cells) relationships between expression of individual glycolytic genes and PD-L1 *H*-score. Gray cells represent absence of a statistically significant correlation. Trends towards positive correlations ($0.05 \le P < 0.10$) are depicted as gray cells labeled with Pearson correlation coefficients. *LAG3*, lymphocyte activating 3; *PDCD1LG2*, programmed cell death 1 ligand 2; *TIGIT*, T cell immunoreceptor with Ig and ITIM domains

genes derived from tumor bulk transcriptome analysis (Fig. 4e) [10]. That analysis revealed statistically significant positive correlations between PD-L1 expression and *ALDOA*, *GAPDH*, *LDHA*, *PFKP*, *PGAM1*, *PGAM4*, and *PGK1* levels (correlation coefficient range $r = 0.292–0.441$). Together, these findings suggest that resected NSCLCs with high glycolytic gene expression and elevated ^{18}F-FDG retention are characterized by enhanced expression of PD-L1.

Recently, we demonstrated that increased tumor glycolytic metabolism impairs T cell trafficking and effector function in NSCLC and melanoma tumors [10]. To evaluate whether noninvasive assessment of tumor glycolysis via ^{18}F-FDG PET could provide a readout of reduced intratumoral immune cell infiltration in resected NSCLCs, we analyzed the correlations between ^{18}F-FDG PET parameters and immune cell populations quantified by IHC in resected tumors. We found that increased ^{18}F-FDG retention, as determined by each PET parameter, was associated with reduced tumor infiltration by $CD57^+$ immune cells (SUV_{Max}, $r = -0.398$, $P = 0.002$; Fig. 4f; SUV_{Mean}, $r = -0.336$, $P = 0.009$; Supplementary Fig. 2a; SUV_{Total}, $r = -0.472$, $P < 0.001$; Supplementary Fig. 2b; TLG, $r = 0.459$, $P < 0.001$; Supplementary Fig. 2c). We further noted inverse correlations between $CD4^+$ immune cell densities and SUV_{Total} ($r = -0.289$, $P = 0.026$) and TLG ($r = -0.295$, $P = 0.023$). Although we did not find clear correlations between ^{18}F-FDG retention and intratumoral infiltration of other immune cells (including $CD8^+$ and $FOXP3^+$ cells), NSCLC tumor samples with elevated glycolytic gene expression and SUV_{Max} had increased expression of transcriptomic signatures suggestive of T cell exhaustion ($r = 0.401$, $P = 0.002$, Fig. 4g; $r = 0.359$, $P = 0.005$, Fig. 4h; $r = 0.302$, $P = 0.020$, Supplementary Fig. 3) [28, 29]. Considered in the context of work revealing a relationship between tumor glycolysis and T cell and natural killer cell hyporesponsiveness [6, 10, 40], the findings from this cohort suggest that highly glycolytic resected NSCLCs are characterized by features indicative of a poorly infiltrated and immunosuppressive phenotype and that noninvasive measurement of tumor ^{18}F-FDG retention according to SUV_{Max} may serve as a potential clinical indicator of these characteristics (Supplementary Fig. 4).

Tumor immunometabolic phenotypes are associated with overall survival in patients with resected NSCLC

Because pretreatment ^{18}F-FDG retention has been identified as an adverse prognostic factor in NSCLCs and other solid tumors [11], we evaluated whether local tumor glycolysis-related changes are associated with prognosis in NSCLC patients and whether ^{18}F-FDG retention could represent a clinical indicator of outcome in our dataset. By analyzing dysregulated genes that were associated with tumor bulk glycolytic gene expression, we identified a gene signature that was upregulated in highly glycolytic tumors (Upregulated Immune Signature of Tumors with High Glycolysis [UISTHG]: *BIRC5*, *F12*, *IL1A*, *PBK*, *TTK*) and a gene signature that was downregulated in NSCLC tumors with high glycolytic gene expression (Downregulated Immune Signature of Tumors with High Glycolysis [DISTHG]: *C4BPA*, *C5*, *DPP4*, *PLA2G1B*).We tested whether these glycolysis-associated immune gene signatures retained prognostic significance after adjusting for tumor histology, stage, and receipt of neoadjuvant and/or adjuvant platinum-based chemotherapy in the PROSPECT cohort. That analysis demonstrated independent associations between increased (> median) UISTHG (adjusted HR 2.22, 95% CI 1.19–4.15, $P = 0.013$, Fig. 5a) and DISTHG (adjusted HR 0.36, 95% CI 0.20–0.64, $P < 0.001$, Fig. 5b) with postoperative OS, as well as with postoperative DFS (UISTHG: adjusted HR 1.61, 95% CI 0.98–2.65, $P = 0.063$; DISTHG: adjusted HR 0.68, 95% CI 0.47–0.97, $P = 0.033$). We next examined whether assessment of ^{18}F-FDG uptake according to SUV_{Max} identified tumor expression of these signatures. We identified a strong positive correlation between SUV_{Max} and UISTHG (Fig. 5c) and an inverse association between SUV_{Max} and DISTHG (Fig. 5d). To provide representative clinical examples of the prognostic significance of ^{18}F-FDG retention as quantified by SUV_{Max} in the PROSPECT cohort, we identified two treatment-naïve patients who underwent complete resection of clinical stage I lung adenocarcinoma (Fig. 5e, f; both resected tumors were pathologic stage I). One patient had a highly hypermetabolic tumor and poor survival (SUV_{Max}, 8.41, Fig. 5e; OS duration, 22 months), whereas the other one had a tumor with low ^{18}F-FDG retention and longer survival following tumor resection (SUV_{Max}, 3.26, Fig. 5f; OS duration, 48 months). Histopathologic examination of the resected tumor samples demonstrated that the immune infiltrate of hypermetabolic tumor (Fig. 5e) was much less than that of the tumor with low ^{18}F-FDG retention (Fig. 5f), further illustrating the association between tumor ^{18}F-FDG retention and tumor immune phenotypes.

Finally, to validate the prognostic significance of these two gene sets (UISTHG, DISTHG) in an independent cohort, we examined publicly available transcriptomic data (compiled from GEO, TCGA, and caArray datasets) [32], which indicated poor prognosis in patients with elevated (> median) UISTHG (Fig. 6a; adjusted HR 1.66, 95% CI 1.30–2.12, $P < 0.001$) and improved prognosis in patients with elevated (> median) DISTHG signatures (Fig. 6b; adjusted HR 0.60, 95% CI 0.46–0.76, $P < 0.001$). Taken together, the results of these analyses support further examinations of the use of preoperative SUV_{Max} as a potential pretreatment means of prognostication and suggest that increased overall tumor glycolytic metabolism, measured

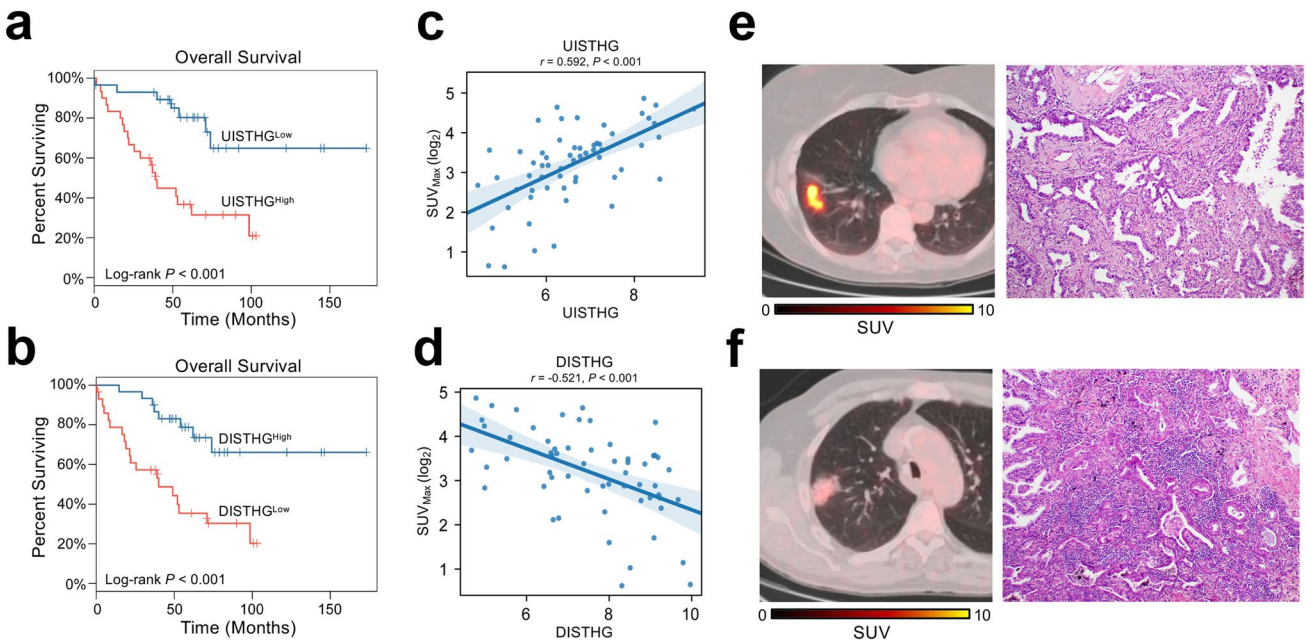

Fig. 5 Preoperative SUV_{Max} correlates with tumor glycolysis-associated immune transcriptomic signatures that are prognostic in NSCLC patients. **a** Reduced overall survival (OS) among NSCLC patients with elevated (> median) overall expression of *BIRC5*, *F12*, *IL1A*, *PBK*, *TTK* (Upregulated Immune Signature of Tumors with High Glycolysis, UISTHG). **b** Improved postoperative OS among NSCLC patients with elevated (> median) overall expression of *C4BPA*, *C5*, *DPP4*, *PLA2G1B* (Downregulated Immune Signature of Tumors with High Glycolysis, DISTHG). *P* values were calculated according to the log-rank test. **c** Pairwise correlation between preoperative SUV_{Max} and the overall expression level of UISTHG. **d** Inverse association between preoperative SUV_{Max} and the overall expression level of DISTHG. Pearson coefficients for pairwise correlations between log_2-transformed values was listed. **e** Representative axial ^{18}F-FDG PET/CT image (left panel) and hematoxylin and eosin staining image of tumor sample (right panel) of a patient with a hypermetabolic (SUV_{Max}, 8.41) adenocarcinoma of the right lower lobe (clinical and pathologic stage I; postoperative OS duration of 22 months). **f** Representative axial ^{18}F-FDG PET/CT image (left panel) and hematoxylin and eosin staining image of tumor sample (right panel) of a patient with hypometabolic (SUV_{Max}, 3.26) adenocarcinoma of the right upper lobe (clinical and pathologic stage I; OS duration of 48 months). Color scale bars indicate intensity of ^{18}F-FDG uptake per voxel according to SUV. *BIRC5*, baculoviral IAP repeat containing 5; *C4BPA*, complement component 4 binding protein alpha; *C5*, complement C5; *DPP4*, dipeptidyl peptidase 4; *F12*, coagulation factor XII; *IL1A*, interleukin 1 alpha; *PBK*, PDZ binding kinase; *PLA2G1B*, phospholipase A1 group IB; *TTK*, TTK protein kinase

according to tumor ^{18}F-FDG uptake by SUV_{Max}, correlates with poor immune cell infiltration and elevated expression of immunosuppressive markers that portended poor prognoses in patients with NSCLC.

Discussion

In this study, we identified a correlation between ^{18}F-FDG PET parameters and tumor metabolic and immune phenotypes in patients with resectable NSCLC by retrospectively analyzing tumor samples and preoperative PET/CT imaging of patients undergoing surgical resection of their tumors. We identified significant associations of ^{18}F-FDG PET parameters with tumor expression of a panel of glycolytic genes previously shown to be associated with a poorly immune-infiltrated tumor phenotype [10]. We also found that increased ^{18}F-FDG PET retention, as quantified by SUV_{Max}, correlated with features associated with tumor progression and immunosuppression. When we stratified patients according to the immunometabolic phenotypes of their tumors, we were able to identify patient subgroups with poorer postoperative survival. Collectively, our results advocate for additional evaluation of PET parameters as potential noninvasive clinical indicators of a highly glycolytic tumor metabolism and an immunosuppressive tumor microenvironment.

Over the past several years, it has become increasingly apparent that metabolic dysregulation is a key driver of oncogenesis and immunoediting [10, 41]. Some tumors may favor glycolysis as a means to meet their metabolic demands despite the presence of adequate oxygen content within the tumor microenvironment [42]. Thus, enhanced glycolytic flux within tumor cells may represent an appealing therapeutic target, and identification of a noninvasive method of assessing the tumor metabolic state remains clinically relevant. Not surprisingly, a variety of imaging modalities using radiolabeled probes to target different metabolic pathways are being explored. However, current technical limitations prohibit ready implementation of

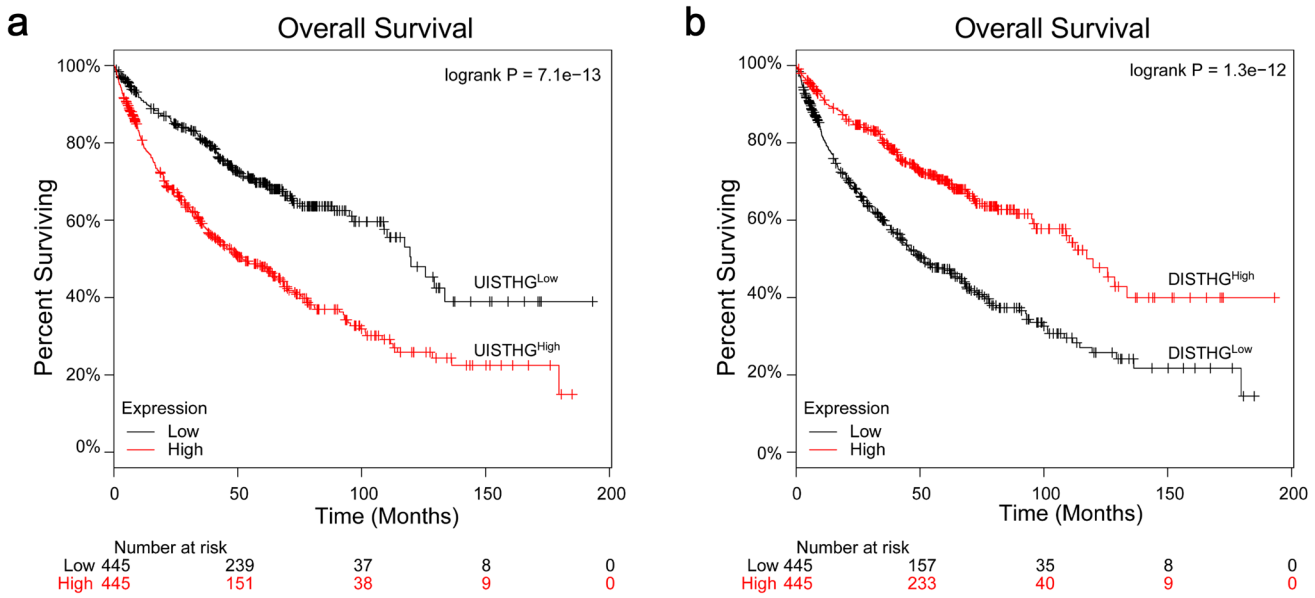

Fig. 6 Prognostic significance of tumor glycolysis-associated immune signatures in NSCLC patients ($n = 890$) according to analysis of publicly available transcriptomic data. **a** Reduced overall survival (OS) among NSCLC patients with elevated (> median) overall expression of UISTHG. **b** Improved postoperative OS among NSCLC patients with elevated (> median) overall expression of DISTHG. *P* values were calculated according to the log-rank test

these experimental modalities in the clinic, and ^{18}F-FDG PET remains the most widely utilized metabolic imaging modality in clinical practice.

Tumor uptake and intracellular sequestration of ^{18}F-FDG are dependent on transmembrane facilitated diffusion, which is mediated by the *SLC2A1* family of transporters and subsequent phosphorylation by hexokinase [43]. Accordingly, much investigative effort has focused on analyzing the relationships between in vivo and in vitro measures of ^{18}F-FDG retention and expression of these proteins in solid tumors [44–47]. However, the relationships between ^{18}F-FDG PET parameters and tumor bulk expression of other glycolysis-related enzymes have not been as fully characterized. Although ^{18}F-FDG PET metabolic parameters identify anatomic areas of enhanced glucose retention and intracellular concentration, whether these parameters can provide information on the actual patterns of intracellular glucose utilization is not well characterized [48, 49]. Here, we identified a positive correlation between increased preoperative ^{18}F-FDG uptake and enhanced tumor bulk glycolysis, as assessed by measuring transcriptome levels of glycolysis-related genes within the tumor tissue, demonstrating that tumors with high ^{18}F-FDG uptake possess elevated expression of genes involved in the glycolytic pathway. Taken in the context of our previous work, which demonstrated that tumor intrinsic glycolysis is associated with the expression of glycolytic genes in melanomas and NSCLCs [10], the results of the present study demonstrate that ^{18}F-FDG PET parameters correlate with tumor glycolysis in resected NSCLC.

By competing for nutrients within the local environment and secreting immunosuppressive metabolites, cancer cells can effectively diminish immune cell trafficking, stimulation, and cytotoxic activity [5–7, 10, 40, 50]. Investigators have demonstrated that tumor infiltration by effector immune cells has prognostic significance in patients with resectable NSCLC [51] and that augmentation of T cell infiltration can be used to overcome resistance to immunotherapies [52]. Consequently, metabolic suppression of the immune response can be expected to have deleterious prognostic effects. Our findings of associations between increased ^{18}F-FDG tumor retention and decreased intratumoral densities of immune cells expressing CD57$^+$ immune cells are consistent with previous reports of inverse correlations between tumor glycolytic metabolism and/or ^{18}F-FDG uptake and tumor infiltration by effector immune cells [14, 40, 53]. Together, our findings indicate that increased ^{18}F-FDG retention may reflect an elevated tumor glycolytic metabolism and an attenuated immune cell-infiltrated tumor microenvironment in patients with resected NSCLC.

Previous mechanistic investigations showed that PD-L1-mediated signaling induces enhanced glycolytic flux in tumors [6]. Therefore, tumor PD-L1 expression contributes to evasion of T cell-mediated adaptive immunity both via direct ligation of PD-1 and promotion of a metabolically unfavorable microenvironment. We found that increased

overall tumor bulk glycolysis, expression of individual glycolytic genes, and noninvasive quantification of tumor glycolytic gene expression by SUV_{Max} are all associated with enhanced expression of PD-L1in resected NSCLCs. These findings suggest that ^{18}F-FDG retention may serve as a potential indicator of tumor PD-L1 expression in NSCLC patients; however, whether this association varies across different stages and hystotypes of NSCLC and after different types of therapies remains to be determined. These data are intriguing in their potential application to identify patients for therapies that target the PD-1/PD-L1 axis, as PD-L1 inhibition suppresses tumor glycolytic metabolism [6]. The extent to which response to various immunotherapies, and their mechanisms of action, is a function of glycolysis-driven tumor immunometabolic features requires additional investigation.

Elevated baseline values of PET parameters have been shown to predict a higher risk of recurrence or death in patients with surgical NSCLC [11, 13]. Also, recent studies suggest that ^{18}F-FDG retention early during treatment with immune checkpoint inhibitors (ICIs) or chemoradiation is an independent factor of poor survival and/or response in patients with locoregionally advanced and metastatic NSCLC [54–56]. In this study, we identified SUV_{Max} as the ^{18}F-FDG PET parameter that is most indicative of glycolysis-associated changes in tumor immune phenotypes. Preoperative SUV_{Max} correlated with tumor bulk gene signatures that were independently associated with survival outcomes, supporting the use of SUV_{Max} as a prognostic factor in our cohort. However, the differences in tumor response to cytotoxic therapy and immunotherapy and their effects on the tumor immune microenvironment are incompletely understood and may depend on several factors, such as tumor molecular and histopathologic features, stage, and prior treatment regimens [57]. As immune-based strategies continue to be explored in the perioperative setting for localized NSCLC [4, 58–60] and gain wider clinical use for metastatic disease [3, 61, 62], further investigations will be needed to delineate the ability of ^{18}F-FDG PET parameters to predict outcomes of these diverse disease groups, with respect to tumor stage, histology, genomic aberrations and prior treatments, as well as responses to ICIs in the perioperative setting for NSCLC and other types of cancer [37, 54, 58]. Also, it should be noted that glucose may not be the only or dominant metabolic fuel utilized by NSCLCs. Faubert et al. recently provided direct evidence that tumor cell-autonomous lactate, rather than glucose, uptake is a major contributor to central metabolism in human NSCLCs with high ^{18}F-FDG PET uptake and aggressive oncological behavior [63]. It remains to be determined whether NSCLCs in different stages and with different biological features and PET retention rely on different substrates as major metabolic fuels.

Using the PROSPECT cohort, which has the unique advantages of full clinical annotation, long follow-up, and comprehensive molecular profiling, we confirmed the prognostic relevance of preoperative ^{18}F-FDG retention in surgically resected tumors and identified two prognostic gene expression signatures. However, our analysis has some limitations that include the biases inherent in a retrospective study design and a bulk tumor mass analysis. First, the gene signatures (UISTHG, DISTHG) identified in the present study were derived from bulk transcriptomic analyses and it is unknown whether the expression levels of individual genes are driven by tumor cells or immune cells. It remains to be determined whether cancer cells or immune cells (or both) are the predominant cell type responsible for the metabolic events depicted by FDG retention in resected NSCLC. A more detailed dissection of the contributions of immune cells and cancer cells to the intratumoral metabolic phenotype requires further studies. Second, metabolic reprogramming in NSCLCs is complex and may be heterogeneous across different histologic subtypes, molecular profiles, and within separate regions of individual tumors [64–66]. Therefore, detailed characterization of immunometabolic differences between NSCLC histologic subtypes, disease stages, tumor genomic features, prior therapies, and the impact of these differences on noninvasive assessment of tumor phenotypes according to ^{18}F-FDG uptake requires investigation in larger cohorts [6–8]. Lastly, we previously identified increased tumor glycolytic metabolism to impact the efficacy of adoptive T cell therapy [10]. However, it is challenging to use gene expression levels to assess tumor glycolytic metabolism in the clinical setting. The goal of our study was to identify potential noninvasive approaches to define the immunometabolic phenotype of tumors. This approach can be potentially used to determine the association between tumor glycolytic features and clinical responses to cancer immunotherapy in future studies. Therefore, in the present work, we focused our analyses on indicators of tumor glycolytic phenotypes. An in-depth radiomic assessment of alternative glucose metabolic pathways will be performed as part of future studies.

In summary, our findings establish that elevated ^{18}F-FDG retention is associated with highly glycolytic metabolism, enhanced PD-L1 expression, and an immunosuppressive phenotype in surgically resected NSCLCs. The results of our study suggest that ^{18}F-FDG PET may serve as a noninvasive clinical indicator of tumor metabolic and immune phenotypes in patients with resectable NSCLC.

Acknowledgements The authors appreciate the assistance of Mr. Alex Liu with the Division of Information Services, Oncology Care and Research IS at MD Anderson Cancer Center, and Mr. Donald Norwood with the Department of Scientific Publications at MD Anderson Cancer Center for his editorial assistance.

Author contributions WP and TC contributed to conception and design. TC, WP, BA, and ERP contributed to development of methodology. TC, WP, BA, KGM, HK, ERP, PV, CB, AR, YW, JW, AW, CAM, and JF contributed to data acquisition. TC, WP, KGM, BA, ERP, PV, CB, AR, YW, AW, JJL, and DPW contributed to analysis and interpretation of data. KGM, BA, BS, MCBG, ERP, PV, HK, CB, AR, AAV, WLH, SGS, WNW, DLG, IIW, PH, JVH, BWC, YW, JW, JJL, DPW, AW, CAM, JF, GLW, DPW, WP, and TC wrote, reviewed, and revised the manuscript. TC, WP, JVH, and IIW contributed to administrative, technical, or material support. WP and TC contributed to study supervision.

Funding This work was supported in part by the National Cancer Institute (5 P50 CA070907; P50 CA221703; R01 CA187076; R01 CA184845, P30CA01667), the Cancer Prevention and Research Institute of Texas (RP170401), the American Society of Clinical Oncology 2018 Career Development Award (12895), the Department of Defense (W81XWH-07-1-0306), and the Bob Mayberry Foundation. This work was also supported in part by the Bruton Endowed Chair in Tumor Biology Funds, and the generous philanthropic contributions to the University of Texas MD Anderson Cancer Center Lung Cancer Moon Shot Program, the Khalifa Scholars Program (from Khalifa Bin Zayed Al Nahyan Foundation), the Advanced Scholar Program (from CG Johnson Foundation), and the Physician Scientist Program (from T.J. Martell Foundation).

Compliance with ethical standards

Conflict of interest M.C.B. Godoy has received research funding from Siemens Healthcare. W.N. William has received honoraria/speaker's fees and/or participated in advisory boards from Roche/Genentech, Bristol-Myers Squibb, Eli Lilly, Merck, AstraZeneca, and Pfizer. D.L. Gibbons has received research funding from AstraZeneca, Janssen, and Takeda and has participated in advisory boards for AstraZeneca and Sanofi. P. Hwu is a consultant and/or has participated in advisory boards for Immatics, Dragonfly, Sanofi, and GlaxoSmithKline. S.G. Swisher has participated in advisory committees for Ethicon and for the Peter MacCallum Cancer Center. B.S. receives consulting fees from Bristol-Myers Squibb. J.V. Heymach has received research support from AstraZeneca, Bayer, GlaxoSmithKline, and Spectrum; participated in advisory committees for AstraZeneca, Boehringer Ingelheim, Exelixis, Genentech, GlaxoSmithKline, Guardant Health, Hengrui, Lilly, Novartis, Specrtum, EMD Serono, and Synta; and received royalties and/or licensing fees from Spectrum. P. Hwu and W. Peng have received research funding in the form of grants to MD Anderson Cancer Center from GlaxoSmith Kline. T. Cascone has received speaker's fees from the Society for Immunotherapy of Cancer and Bristol-Myers Squibb; receives consulting/advisory role fees from MedImmune, Bristol-Myers Squibb and EMD Serono, and research funding to MD Anderson Cancer Center from Boehringer Ingelheim, MedImmune and Bristol-Myers Squibb. No potential conflicts of interest are disclosed by the other authors.

Ethical approval The study was approved by The University of Texas MD Anderson Cancer Center's Institutional Review Board (PROSPECT—LAB07-0233).

Human and animal rights All human studies were conducted in accordance with the Declaration of Helsinki.

Informed consent Informed consent was obtained from all study participants.

References

1. Borghaei H, Paz-Ares L, Horn L et al (2015) Nivolumab versus docetaxel in advanced nonsquamous non-small-cell lung cancer. N Engl J Med 373:1627–1639. https://doi.org/10.1056/NEJMoa1507643
2. Brahmer J, Reckamp KL, Baas P et al (2015) Nivolumab versus docetaxel in advanced squamous-cell non–small-cell lung cancer. N Engl J Med 373:123–135. https://doi.org/10.1056/NEJMoa1504627
3. Reck M, Rodriguez-Abreu D, Robinson AG et al (2016) Pembrolizumab versus chemotherapy for PD-L1-positive non-small-cell lung cancer. N Engl J Med 375:1823–1833. https://doi.org/10.1056/NEJMoa1606774
4. Forde PM, Chaft JE, Smith KN et al (2018) Neoadjuvant PD-1 blockade in resectable lung cancer. N Engl J Med 378:1976–1986. https://doi.org/10.1056/NEJMoa1716078
5. Renner K, Singer K, Koehl GE, Geissler EK, Peter K, Siska PJ, Kreutz M (2017) Metabolic hallmarks of tumor and immune cells in the tumor microenvironment. Front Immunol. https://doi.org/10.3389/fimmu.2017.00248
6. Chang C-H, Qiu J, O'Sullivan D et al (2015) Metabolic competition in the tumor microenvironment is a driver of cancer progression. Cell 162:1229–1241. https://doi.org/10.1016/j.cell.2015.08.016
7. Fischer K, Hoffmann P, Voelkl S et al (2007) Inhibitory effect of tumor cell–derived lactic acid on human T cells. Blood 109:3812–3819. https://doi.org/10.1182/blood-2006-07-035972
8. Estrella V, Chen T, Lloyd M et al (2013) Acidity generated by the tumor microenvironment drives local invasion. Cancer Res 73:1524–1535. https://doi.org/10.1158/0008-5472.can-12-2796
9. Walenta S, Wetterling M, Lehrke M, Schwickert G, Sundfør K, Rofstad EK, Mueller-Klieser W (2000) High lactate levels predict likelihood of metastases, tumor recurrence, and restricted patient survival in human cervical cancers. Cancer Res 60:916–921
10. Cascone T, McKenzie JA, Mbofung RM et al (2018) Increased tumor glycolysis characterizes immune resistance to adoptive T cell therapy. Cell Metab 27:977–87.e4. https://doi.org/10.1016/j.cmet.2018.02.024
11. Liu J, Dong M, Sun X, Li W, Xing L, Yu J (2016) Prognostic value of ^{18}F-FDG PET/CT in surgical non-small cell lung cancer: a meta-analysis. PLoS ONE 11:e0146195. https://doi.org/10.1371/journal.pone.0146195
12. Pak K, Cheon GJ, Nam HY, Kim SJ, Kang KW, Chung JK, Kim EE, Lee DS (2014) Prognostic value of metabolic tumor volume and total lesion glycolysis in head and neck cancer: A systematic review and meta-analysis. J Nucl Med 55:884–890. https://doi.org/10.2967/jnumed.113.133801
13. Im HJ, Pak K, Cheon GJ, Kang KW, Kim SJ, Kim IJ, Chung JK, Kim EE, Lee DS (2015) Prognostic value of volumetric parameters of ^{18}F-FDG PET in non-small-cell lung cancer: a meta-analysis. Eur J Nucl Med Mol Imaging 42:241–251. https://doi.org/10.1007/s00259-014-2903-7
14. Kwon HR, Pahk K, Park S et al (2019) Prognostic value of metabolic information in advanced gastric cancer using preoperative (18)F-FDG PET/CT. Nucl Med Mol Imaging 53:386–395. https://doi.org/10.1007/s13139-019-00622-w
15. Bruzzi JF, Munden RF (2006) PET/CT imaging of lung cancer. J Thorac Imaging 21:123–136
16. Cardnell RJG, Behrens C, Diao L et al (2015) An integrated molecular analysis of lung adenocarcinomas identifies potential therapeutic targets among TTF1-negative tumors, including DNA repair proteins and Nrf2. Clin Cancer Res 21:3480–3491. https://doi.org/10.1158/1078-0432.ccr-14-3286

17. Skoulidis F, Byers LA, Diao L et al (2015) Co-occurring genomic alterations define major subsets of *KRAS*-mutant lung adenocarcinoma with distinct biology, immune profiles, and therapeutic vulnerabilities. Cancer Discov 5:860–877. https://doi.org/10.1158/2159-8290.cd-14-1236
18. Tang H, Xiao G, Behrens C et al (2013) A 12-gene set predicts survival benefits from adjuvant chemotherapy in non-small cell lung cancer patients. Clin Cancer Res 19:1577–1586. https://doi.org/10.1158/1078-0432.ccr-12-2321
19. Mohammed N, Kestin LL, Grills IS, Battu M, Fitch DL, C-yO W, Margolis JH, Chmielewski GW, Welsh RJ (2011) Rapid disease progression with delay in treatment of non–small-cell lung cancer. Int J Radiat Oncol Biol Phys 79:466–472. https://doi.org/10.1016/j.ijrobp.2009.11.029
20. Goldstraw P, Crowley J, Chansky K, Giroux DJ, Groome PA, Rami-Porta R, Postmus PE, Rusch V, Sobin L (2007) The IASLC lung cancer staging project: proposals for the revision of the TNM stage groupings in the forthcoming (seventh) edition of the TNM Classification of malignant tumours. J Thorac Oncol 2:706–714. https://doi.org/10.1097/JTO.0b013e31812f3c1a
21. Mhlanga JC, Chirindel A, Lodge MA, Wahl RL, Subramaniam RM (2018) Quantitative PET/CT in clinical practice: assessing the agreement of PET tumor indices using different clinical reading platforms. Nucl Med Commun 39:154–160. https://doi.org/10.1097/mnm.0000000000000786
22. Werner-Wasik M, Nelson AD, Choi W et al (2012) What is the best way to contour lung tumors on PET scans? Multiobserver validation of a gradient-based method using a NSCLC digital PET phantom. Int J Radiat Oncol Biol Phys 82:1164–1171. https://doi.org/10.1016/j.ijrobp.2010.12.055
23. Nilsson MB, Sun H, Diao L et al (2017) Stress hormones promote EGFR inhibitor resistance in NSCLC: implications for combinations with beta-blockers. Sci Transl Med. https://doi.org/10.1126/scitranslmed.aao4307
24. Cesano A (2015) nCounter® PanCancer immune profiling panel (NanoString Technologies Inc, Seattle, WA). J Immunother Cancer 3:42. https://doi.org/10.1186/s40425-015-0088-7
25. Benjamini Y, Hochberg Y (1995) Controlling the false discovery rate: a practical and powerful spproach to multiple testing. J R Stat Soc Ser B (Methodological) 57:289–300
26. Law CW, Alhamdoosh M, Su S, Dong X, Tian L, Smyth GK, Ritchie ME (2016) RNA-seq analysis is easy as 1-2-3 with limma, Glimma and edgeR. F1000Res. https://doi.org/10.12688/f1000research.9005.3
27. Krämer A, Green J, Pollard J Jr, Tugendreich S (2013) Causal analysis approaches in ingenuity pathway analysis. Bioinformatics 30:523–530. https://doi.org/10.1093/bioinformatics/btt703
28. Danaher P, Warren S, Lu R, Samayoa J, Sullivan A, Pekker I, Wallden B, Marincola FM, Cesano A (2018) Pan-cancer adaptive immune resistance as defined by the tumor inflammation signature (TIS): results from the cancer genome atlas (TCGA). J Immunother Cancer 6:63. https://doi.org/10.1186/s40425-018-0367-1
29. Jerby-Arnon L, Shah P, Cuoco MS et al (2018) A cancer cell program promotes T cell exclusion and resistance to checkpoint blockade. Cell 175:984–97.e24. https://doi.org/10.1016/j.cell.2018.09.006
30. Parra ER, Behrens C, Rodriguez-Canales J et al (2016) Image analysis-based assessment of PD-L1 and tumor-associated immune cells density supports distinct intratumoral microenvironment groups in non-small cell lung carcinoma patients. Clin Cancer Res 22:6278–6289. https://doi.org/10.1158/1078-0432.ccr-15-2443
31. Kadara H, Choi M, Zhang J et al (2017) Whole-exome sequencing and immune profiling of early-stage lung adenocarcinoma with fully annotated clinical follow-up. Ann Oncol 28:75–82. https://doi.org/10.1093/annonc/mdw436
32. Győrffy B, Surowiak P, Budczies J, Lánczky A (2013) Online survival analysis software to assess the prognostic value of biomarkers using transcriptomic data in non-small-cell lung cancer. PLoS ONE 8:e82241. https://doi.org/10.1371/journal.pone.0082241
33. R Core Team R: A language and environment for statistical computing. R Foundation for Statistical Computing. Vienna, Austria. https://www.R-project.org/.
34. Chung AS, Wu X, Zhuang G et al (2013) An interleukin-17–mediated paracrine network promotes tumor resistance to anti-angiogenic therapy. Nat Med 19:1114. https://doi.org/10.1038/nm.3291
35. Charles KA, Kulbe H, Soper R et al (2009) The tumor-promoting actions of TNF-alpha involve TNFR1 and IL-17 in ovarian cancer in mice and humans. J Clin Invest 119:3011–3023. https://doi.org/10.1172/jci39065
36. Alfaro C, Teijeira A, Oñate C et al (2016) Tumor-produced interleukin-8 attracts human myeloid-derived suppressor cells and elicits extrusion of neutrophil extracellular traps (NETs). Clin Cancer Res 22:3924–3936. https://doi.org/10.1158/1078-0432.Ccr-15-2463
37. Wellenstein MD, de Visser KE (2018) Cancer-cell-intrinsic mechanisms shaping the tumor immune landscape. Immunity 48:399–416. https://doi.org/10.1016/j.immuni.2018.03.004
38. Liu J, Zhang C, Wu R, Lin M, Liang Y, Liu J, Wang X, Yang B, Feng Z (2015) RRAD inhibits the Warburg effect through negative regulation of the NF-KB signaling. Oncotarget 6:14982–14992. https://doi.org/10.18632/oncotarget.3719
39. Wang H, Nicolay BN, Chick JM et al (2017) The metabolic function of cyclin D3–CDK6 kinase in cancer cell survival. Nature 546:426. https://doi.org/10.1038/nature22797
40. Brand A, Singer K, Koehl Gudrun E et al (2016) LDHA-associated lactic acid production blunts tumor immunosurveillance by T and NK cells. Cell Metab 24:657–671. https://doi.org/10.1016/j.cmet.2016.08.011
41. Vander Heiden MG, DeBerardinis RJ (2017) Understanding the intersections between metabolism and cancer biology. Cell 168:657–669. https://doi.org/10.1016/j.cell.2016.12.039
42. Vander Heiden MG, Cantley LC, Thompson CB (2009) Understanding the Warburg effect: the metabolic requirements of cell proliferation. Science 324:1029–1033. https://doi.org/10.1126/science.1160809
43. Timm KN, Kennedy BW, Brindle KM (2016) Imaging tumor metabolism to assess disease progression and treatment response. Clin Cancer Res 22:5196–5203. https://doi.org/10.1158/1078-0432.ccr-16-0159
44. Mamede M, Higashi T, Kitaichi M et al (2005) ^{18}F-FDG Uptake and PCNA, Glut-1, and Hexokinase-II expressions in cancers and inflammatory lesions of the lung. Neoplasia (New York, N. Y.) 7:369–379. https://doi.org/10.1593/neo.04577
45. Kaira K, Serizawa M, Koh Y et al (2014) Biological significance of ^{18}F-FDG uptake on PET in patients with non-small-cell lung cancer. Lung Cancer 83:197–204. https://doi.org/10.1016/j.lungcan.2013.11.025
46. Zhou X, Chen R, Xie W, Ni Y, Liu J, Huang G (2014) Relationship between ^{18}F-FDG accumulation and lactate dehydrogenase A expression in lung adenocarcinomas. J Nucl Med 55:1766–1771. https://doi.org/10.2967/jnumed.114.145490
47. Goodwin J, Neugent ML, Lee SY et al (2017) The distinct metabolic phenotype of lung squamous cell carcinoma defines selective vulnerability to glycolytic inhibition. Nat Commun 8:15503. https://doi.org/10.1038/ncomms15503
48. Boroughs LK, DeBerardinis RJ (2015) Metabolic pathways promoting cancer cell survival and growth. Nat Cell Biol 17:351. https://doi.org/10.1038/ncb3124

49. Contractor KB, Aboagye EO (2009) Monitoring predominantly cytostatic treatment response with ^{18}F-FDG PET. J Nucl Med 50:97S–105S. https://doi.org/10.2967/jnumed.108.057273
50. Ottensmeier CH, Perry KL, Harden EL et al (2016) Upregulated glucose metabolism correlates inversely with CD8$^+$ T-cell infiltration and survival in squamous cell carcinoma. Cancer Res 76:4136–4148. https://doi.org/10.1158/0008-5472.can-15-3121
51. Soo RA, Chen Z, Yan Teng RS, Tan HL, Iacopetta B, Tai BC, Soong R (2018) Prognostic significance of immune cells in non-small cell lung cancer: meta-analysis. Oncotarget 9:24801–24820. https://doi.org/10.18632/oncotarget.24835
52. Tang H, Wang Y, Chlewicki LK, Zhang Y, Guo J, Liang W, Wang J, Wang X, Fu Y-X (2016) Facilitating T cell infiltration in tumor microenvironment overcomes resistance to PD-L1 blockade. Cancer Cell 29:285–296. https://doi.org/10.1016/j.ccell.2016.02.004
53. Lopci E, Toschi L, Grizzi F et al (2016) Correlation of metabolic information on FDG-PET with tissue expression of immune markers in patients with non-small cell lung cancer (NSCLC) who are candidates for upfront surgery. Eur J Nucl Med Mol Imaging 43:1954–1961. https://doi.org/10.1007/s00259-016-3425-2
54. Kaira K, Higuchi T, Naruse I et al (2018) Metabolic activity by (18)F-FDG-PET/CT is predictive of early response after nivolumab in previously treated NSCLC. Eur J Nucl Med Mol Imaging 45:56–66. https://doi.org/10.1007/s00259-017-3806-1
55. Usmanij EA, de Geus-Oei LF, Troost EG, Peters-Bax L, van der Heijden EH, Kaanders JH, Oyen WJ, Schuurbiers OC, Bussink J (2013) ^{18}F-FDG PET early response evaluation of locally advanced non-small cell lung cancer treated with concomitant chemoradiotherapy. J Nucl Med 54:1528–1534. https://doi.org/10.2967/jnumed.112.116921
56. Spigel DRCJ, Gettinger S, Chao BH, Dirix L, Schmid P et al (2018) FIR: Efficacy, safety, and biomarker analysis of a phase II open-label study of atezolizumab in PD-L1-selected patients with NSCLC. J Thorac Oncol 13:1733–1742
57. Parra ER, Villalobos P, Behrens C et al (2018) Effect of neoadjuvant chemotherapy on the immune microenvironment in non-small cell lung carcinomas as determined by multiplex immunofluorescence and image analysis approaches. J Immunother Cancer 6:48. https://doi.org/10.1186/s40425-018-0368-0
58. Cascone T, William WN, Weissferdt A et al (2019) Neoadjuvant nivolumab (N) or nivolumab plus ipilimumab (NI) for resectable non-small cell lung cancer (NSCLC): Clinical and correlative results from the NEOSTAR study. J Clin Oncol 37: suppl; abstr 8504. https://doi.org/10.1200/JCO.2019.37.15_suppl.8504
59. Kwiatkowski DJ, Rusch VR, Chaft JE et al (2019) Neoadjuvant atezolizumab in resectable non-small cell lung cancer (NSCLC): interim analysis and biomarker data from a multicenter study (LCMC3). J Clin Oncol 37: suppl; abstr 8503. https://doi.org/10.1200/JCO.2019.37.15_suppl.8503
60. Provenico M, Nadal E, Insa A et al (2019) Neoadjuvant chemoimmunotherapy for the treatment of stage IIIA resectable non-small cell lung cancer (NSCLC): a phase II multicenter exploratory study-Final data of patients who underwent surgical assessment. J Clin Oncol 37: suppl; abstr 8509. https://doi.org/10.1200/JCO.2019.37.15_suppl.8509
61. Gandhi L, Rodríguez-Abreu D, Gadgeel S et al (2018) Pembrolizumab plus chemotherapy in metastatic non–small-cell lung cancer. N Engl J Med 378:2078–2092. https://doi.org/10.1056/NEJMoa1801005
62. Lopes G, Wu Y-L, Kudaba I et al. (2018) Pembrolizumab (pembro) versus platinum-based chemotherapy (chemo) as first-line therapy for advanced/metastatic NSCLC with a PD-L1 tumor proportion score (TPS) ≥ 1%: Open-label, phase 3 KEYNOTE-042 study. J Clin Oncol. 36: LBA4-LBA. https://doi.org/10.1200/JCO.2018.36.18_suppl.LBA4
63. Faubert B, Li KY, Cai L et al (2017) Lactate metabolism in human lung tumors. Cell 171:358–371. https://doi.org/10.1016/j.cell.2017.09.019
64. Momcilovic M, Jones A, Bailey ST et al (2019) In vivo imaging of mitochondrial membrane potential in non-small-cell lung cancer. Nature 575:380–384. https://doi.org/10.1038/s41586-019-1715-0
65. Hensley CT, Faubert B, Yuan Q et al (2016) Metabolic heterogeneity in human lung tumors. Cell 164:681–694. https://doi.org/10.1016/j.cell.2015.12.034
66. Chen PH, Cai L, Huffman K et al (2019) Metabolic diversity in human non-small cell lung cancer cells. Mol Cell 76:838–51.e5. https://doi.org/10.1016/j.molcel.2019.08.028

Affiliations

Kyle G. Mitchell[1] · Behrang Amini[2] · Yunfei Wang[3] · Brett W. Carter[2] · Myrna C. B. Godoy[2] · Edwin R. Parra[4] · Carmen Behrens[5] · Pamela Villalobos[4] · Alexandre Reuben[5] · J. Jack Lee[6] · Annikka Weissferdt[7] · Cesar A. Moran[7] · Junya Fujimoto[4] · Boris Sepesi[1] · Garrett L. Walsh[1] · Ara A. Vaporciyan[1] · Wayne L. Hofstetter[1] · William N. William Jr.[5,8] · Don L. Gibbons[5,9] · Jing Wang[10] · Patrick Hwu[3] · Stephen G. Swisher[1] · David Piwnica-Worms[11] · Humam Kadara[4] · Ignacio I. Wistuba[4,5] · John V. Heymach[5] · Weiyi Peng[3,12] · Tina Cascone[5]

1 Department of Thoracic and Cardiovascular Surgery, The University of Texas MD Anderson Cancer Center, Houston, TX, USA

2 Department of Diagnostic Radiology, The University of Texas MD Anderson Cancer Center, Houston, TX, USA

3 Department of Melanoma Medical Oncology, The University of Texas MD Anderson Cancer Center, Houston, TX, USA

4 Department of Translational Molecular Pathology, The University of Texas MD Anderson Cancer Center, Houston, TX, USA

5 Department of Thoracic/Head and Neck Medical Oncology, The University of Texas MD Anderson Cancer Center, 1515 Holcombe Blvd, Unit 432, Houston, TX 77030, USA

[6] Department of Biostatistics, The University of Texas MD Anderson Cancer Center, Houston, TX, USA

[7] Department of Pathology, The University of Texas MD Anderson Cancer Center, Houston, TX, USA

[8] Hospital BP, a Beneficencia Portuguesa de Sao Paulo, Sao Paulo, Brazil

[9] Department of Molecular and Cellular Oncology, The University of Texas MD Anderson Cancer Center, Houston, TX, USA

[10] Department of Bioinformatics and Computational Biology, The University of Texas MD Anderson Cancer Center, Houston, TX, USA

[11] Department of Cancer Systems Imaging, The University of Texas MD Anderson Cancer Center, Houston, TX, USA

[12] Department of Biology and Biochemistry, The University of Houston, 3517 Cullen Blvd., Houston, TX 77204, USA